

Study on the space frame structures incorporated with magnetorheological dampers

Fei-Hong Xu¹, Zhao-Dong Xu^{*1} and Xiang-Cheng Zhang²

¹Key Laboratory of C&PC Structures of the Ministry of Education, Southeast University, Nanjing, 210096, Jiangsu, P.R. China

²School of Mechanics and Engineering Science, Zhengzhou University, Zhengzhou, 450001, Henan, P.R. China

(Received September 12, 2015, Revised November 13, 2016, Accepted January 3, 2017)

Abstract. Magnetorheological damper has received significant attention in recent years due to the reason that it can offer adaptability of active control devices without requiring the associated large power sources. In this paper, performance tests on a MR damper are carried out under different currents, excitation amplitudes and frequencies, the damping characteristics and energy dissipation capacity of the MR damper are analyzed. Elasto-plastic dynamic analysis on a space frame structure incorporated with MR dampers is conducted, and numerical analysis results show that MR dampers can significantly mitigate the structural vibration responses. Finally, the genetic algorithm with the improved binary crossover and mutation technique is adopted to optimize the arrangement of MR dampers. Numerical results show that dynamic responses of the optimal controlled structure are mitigated more effectively.

Keywords: magnetorheological damper; performance test; elasto-plastic analysis; genetic algorithm; optimization

1. Introduction

Structural vibration control is an effective way by using the control device to mitigate the vibration energy and reduce the response of structure under seismic and wind excitations (Soong and Cimellaro 2009, Xu *et al.* 2016a, b, c). Till now, magnetorheological (MR) damper, as a semi-active control device, has been paid more and more attention by researchers (Spencer *et al.* 1997, Tu *et al.* 2011). The first 200kN full-scale MR damper was designed and fabricated by Lord Company (Carlson *et al.* 1996), and then a series of experimental and theoretical study have been carried out by researchers (Jansen and Dyke 2000, Xu and Shen 2003, Xu *et al.* 2003, Kim *et al.* 2009, Cetin *et al.* 2011, Yan *et al.* 2011).

Due to the complex rheological properties of MR dampers, the general finite element software cannot simulate the mechanical properties of MR damper effectively, which makes it difficult to calculate the dynamic responses of structures incorporated with MR dampers. Thus programming is the available method to solve this problem, and then a reasonable mathematical model is needed to describe the properties of MR dampers. In order to describe the behaviors of MR dampers, many mathematical models are proposed, these models of MR dampers can be classified into two main categories, which are the quasi-static model and dynamic model. The most classic quasi-static model of MR damper was proposed by Phillips, which was deduced according to the Navier-Stokes equations based on the parallel plate model (Phillips 1969).

Then some other quasi-static models were put forward successively by other researchers (Wereley and Pang 1998, Wang and Gordaninejad 1999, Lee and Wereley 1999, Yang *et al.* 2002). However, the quasi-static model cannot describe the hysteretic characteristics of force-velocity curves, thus dynamic models are put forward (Spencer *et al.* 1997, Jansen and Dyke 2000, Xu *et al.* 2012), and these models are parametric models and need sufficient test data to identify the parameters.

Based on the mathematical model of MR dampers, dynamic responses of the structures incorporated with MR dampers can be calculated. In terms of building structure, the story shear model (Motra *et al.* 2011, Tsang *et al.* 2006, Xu and Guo 2006) is widely used to calculate the dynamic responses of frame structures. However, elasto-plastic deformation will be produced under strong earthquake excitations, while the story shear model is so simplified that cannot reflect the failure mechanism of structures. Thus further researches on the establishment of a more accurate model based on space element model for the frame structure are very necessary.

In this study, performance test on the MR damper is carried out under different currents, excitation amplitudes and frequencies, and the energy dissipation capacity of the MR damper is also analyzed. Then the general elasto-plastic dynamic analysis program for space frame structure incorporated with MR dampers is developed based on the space element model using MATLAB, this program can calculate the dynamic responses of magnetorheological damping structures effectively and quickly. In order to obtain the optimal control effect, the locations of MR dampers are optimized by using genetic algorithm. The optimal locations under different determinate number of MR dampers are obtained. Comparison results show that the dynamic responses of optimized magnetorheological

*Corresponding author, Professor
E-mail: xuzhdgyq@seu.edu.cn

damping structure are mitigated more effectively.

2. Experimental study on MR damper

The designed MR damper in this study is shown in Fig. 1, which is a shear valve MR damper. When the piston moves due to the relative motion of the structure under external excitation, on the one hand, the MR fluid will be subjected to shear force due to the motion of both the piston and the inner cylinder; on the other hand, the MR fluid will flow from one chamber to the other chamber due to the pressure drop generated by the motion of piston. These two aspects will both provide damping force.

In order to realize large damping force, five-stage coils are adopted here, which can not only extend the effective damping gap and then provide large damping force, but also make the magnetic field distribution more uniform. The corresponding sizes of each part of the damper are listed in Table 1. Before calculating the dynamic responses of structures incorporated with MR dampers, the damping force range of the MR damper should be determined firstly, thus Performance test on this damper is conducted and the detailed test procedure and results are discussed in the following.

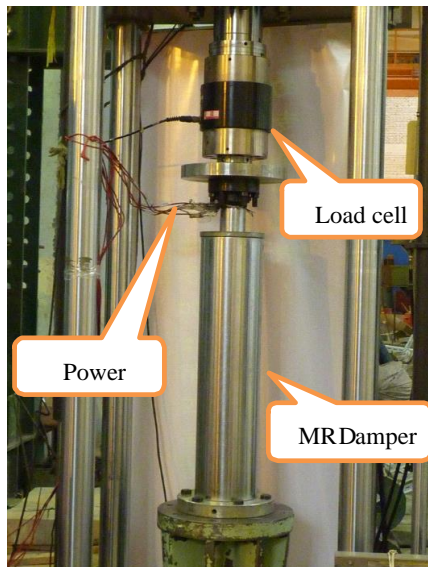


Fig. 1 Testing of MR damper

Table 1 Geometric parameters of MR damper

parameter	Size	parameter	Size
Inner diameter of cylinder (mm)	194	Piston diameter (mm)	156
Outer diameter of cylinder (mm)	460	Piston length (mm)	500
Magnetic core diameter (mm)	110	Effective piston length (mm)	250
Stroke (mm)	50	Damping gap (mm)	2
Piston rod diameter (mm)	80	Current range (A)	0-3
MR damper length (mm)	1150	Coil (n×turns)	5×840

Table 2 Loading cases of the MR damper

Current (A)	Loading amplitudes under different frequencies (mm)			Cycles
	0.1, 0.2 Hz	0.5 Hz	1.0Hz	
0	10,20,30,40	5,10,20,30	5,10,20	20
0.6	10,20,30,40	5,10,20,30	5,10,20	20
1.2	10,20,30,40	5,10,20,30	5,10,20	20
1.8	10,20,30,40	5,10,20,30	5,10,20	20
2.1	10,20,30,40	5,10,20,30	5,10,20	20
2.4	10,20,30,40	5,10,20,30	5,10,20	20

2.1 Test description

The test is conducted using a 1000 kN MTS electro-hydraulic servo material testing machine, as shown in Fig. 1. During the test, the dynamic loading is applied via the actuator of the loading device and a sinusoidal excitation is chosen. The sinusoidal wave can be expressed as $u_d = u_0 \sin(2\pi ft)$, where u_0 is the loading displacement amplitude, f is the loading frequency, and t is the loading time. The loading cases are listed in Table 2.

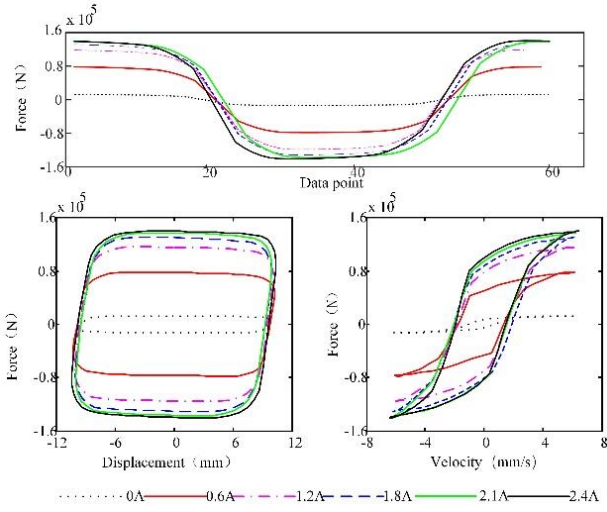
2.2 Results and analysis

Based on the test results, the force-displacement and force-velocity hysteresis curves are plotted, as seen in Fig. 2, respectively. Fig. 2(a) shows the hysteresis curves under different currents with the amplitude of 10 mm and frequency 0.2 Hz, it can be seen that the damping force changes significantly when the current increases from 0 A to 1.8 A, the values of damping force are 12.93 kN, 77.81 kN, 116.28 kN and 131.66 kN, respectively. While the damping force increment is not obvious when the current exceeds 1.8 A, the damping forces are 137.84 kN and 140.85kN respectively, which verified the existence of magnetic saturation of MR dampers. The minimum damping force F_v is approximately 12.93 kN, and the maximum force F_{max} under 2.4 A is approximately 140.1 kN. Then the adjusting coefficient of the MR damper $K = F_\tau / F_v = (F_{max} - F_v) / F_v$ is 9.84 This adjusting coefficient is relatively large and it implies that the MR damper has a large adjusting range, which will make a good contribution to structural vibration control.

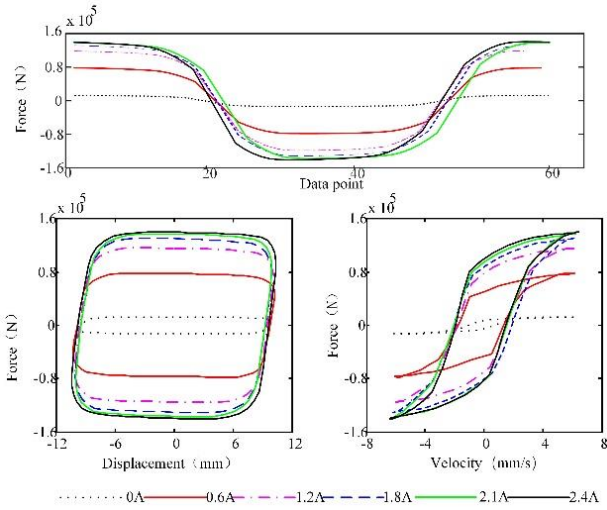
Fig. 2(b) shows the hysteresis curves under different amplitudes with the current of 1.2A and frequency 0.2Hz, it can be seen that the damping force increases slightly with increasing amplitudes. Similarly, Fig. 2(c) shows the hysteresis curves under different frequencies with the current of 1.2A and the amplitude of 10mm, it can be also seen that the damping force also changes slightly with increasing frequency. These results indicate that the influence of excitation amplitude and frequency on the damping force of MR damper is very limited and inconspicuous. However, as seen from the force-velocity curves, the width of the hysteretic loop at the lower velocity region increase with increasing amplitudes and frequencies, which means that the nonlinear characteristics becomes

more obvious.

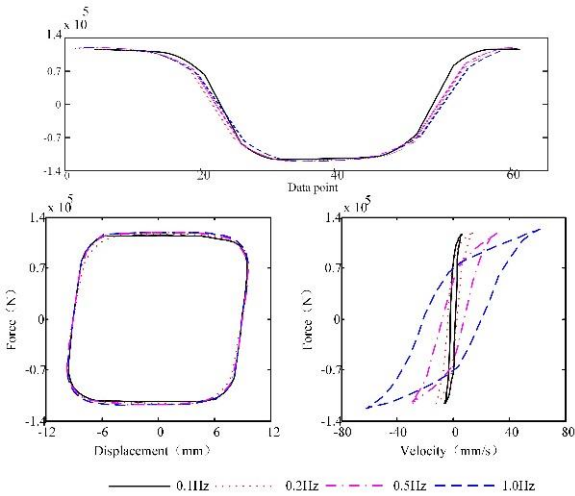
The energy dissipation capacity of the MR damper is also analyzed, generally, the energy dissipation E_d can be



(a) Hysteresis curves under different currents

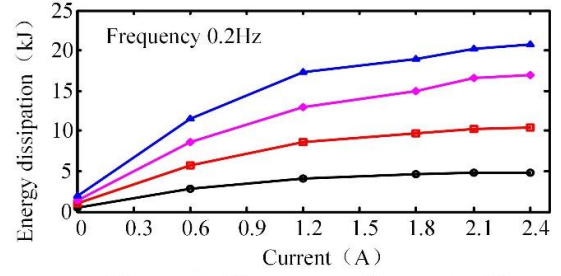


(b) Hysteresis curves under different loading amplitudes

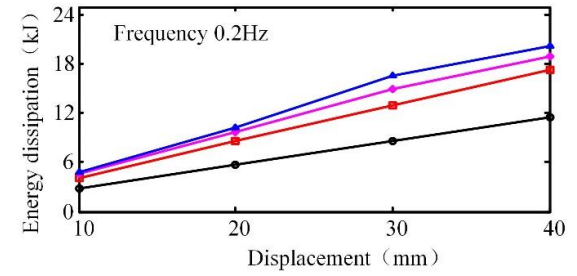


(c) Hysteresis curves under different loading frequencies

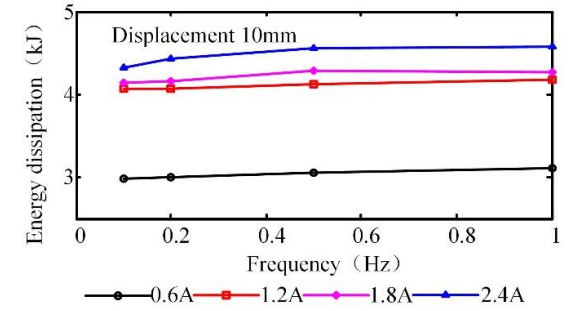
Fig. 2 Hysteresis curves of the MR damper under different condition



(a) Energy dissipation with varying current



(b) Energy dissipation with varying loading amplitude



(c) Energy dissipation with varying loading frequency

Fig. 3 Energy dissipation of the MR damper under different condition

calculated by calculating the area enclosed by the force-displacement hysteresis curves, and then E_d is given by

$$E_d = \int F(t)du = \int_0^{2\pi/\omega} F(t)\dot{u}(t)dt \quad (1)$$

where, $F(t)$ is the damping force of the MR damper, $\dot{u}(t)$ is the velocity of the piston, ω is the loading frequency.

The results are shown in Fig. 3. Fig. 3(a) shows the energy dissipation with increasing current under different displacements, the frequency is 0.2 Hz, it can be seen that the energy dissipation increases dramatically with increasing current and finally almost maintain the same at the scope of magnetic saturation. Specifically, when the displacement is 10 mm, the energy dissipation values are 0.46 kJ, 2.78 kJ, 4.07 kJ, 4.62 kJ, 4.78 kJ and 4.81 kJ, respectively. When the current exceeds 2.1 A, the energy dissipation shows minimal growth. Fig. 3(b) shows the energy dissipation with increasing loading amplitude under different currents, the frequency is 0.2 Hz, it can be seen that the energy dissipation increases linearly with varying amplitudes. For instance, when the current is 1.2 A, the

energy dissipation values are 4.08 kJ, 8.53 kJ, 12.89 kJ and 17.35 kJ, respectively. Fig. 3(c) shows the energy dissipation with increasing loading frequency under different currents, the displacement is 10 mm, it can be seen that the energy dissipation nearly maintain the same with increasing frequency, taking 1.2 A of the current for example, the energy dissipation values are 4.07 kJ, 4.08 kJ, 4.12 kJ and 4.17 kJ, respectively. The above results indicate that current and amplitude affect the energy dissipation capacity significantly, and the frequency almost has little contribution to the energy dissipation capacity.

3. Elasto-plastic dynamic analysis

In order to verify the control effect of MR dampers and prepare for the optimization analysis, the elasto-plastic dynamic analyses of space frame structure incorporated with MR dampers are carried out in this section, detailed discussions are shown as following.

3.1 Motion equation of the controlled structure

MR dampers are usually installed between the column support and beam column joints of the structure, under the external excitation, the displacement between storeys will lead to the motion of the damper and dissipate vibration energy, the motion equation of the controlled structure can be written as following.

$$[M]\{\ddot{X}\} + [C]\{\dot{X}\} + [K]\{X\} = -[M]\{1\}\ddot{X}_g - [H]\{U\} \quad (2)$$

where $[M]$, $[K]$, $[C]$ are the mass matrix, stiffness matrix and damping matrix, $\{1\}$ is the unit column vector, $[H]$ is the location matrix of MR dampers, $\{U\}$ is the control force vector of the MR dampers, \ddot{X}_g is the seismic acceleration, $\{X\}$ is the displacement vector of the structure.

When the structure is subjected to strong earthquake excitation, elasto-plastic deformation will be produced at the end of the structure member, thus the elasto-plastic dynamic analysis is needed. In order to analyze the structural elasto-plastic response, the elasto-plastic stiffness matrix of the member should be determined firstly. Taking the bending deformation in the XZ plane for example, according to the Giberson single component model (Giberson 1969), the inflection point is assumed to be located in the middle of the member, then the rotation increment of the two ends are equal. Thus the bending moment increment at the i th end of the member can be obtained using the following equation,

$$\Delta M_i = S_{ij}(\Delta\theta_i - \Delta\alpha_i) + S_{ji}(\Delta\theta_j - \Delta\alpha_j) = K_{0i}(\Delta\theta_i - \Delta\alpha_i) \quad (3)$$

where S_{ij} and S_{ji} are the flexural rigidity considering the shear deformation. $\Delta\theta$ and $\Delta\alpha$ are the angle increment and plastic angle increment of the member end, respectively, K_{0i} is the equivalent bending stiffness of the end i .

According to the restoring force characteristics of the member, as shown in Fig. 4, the plastic rotation angle increment can be obtained as

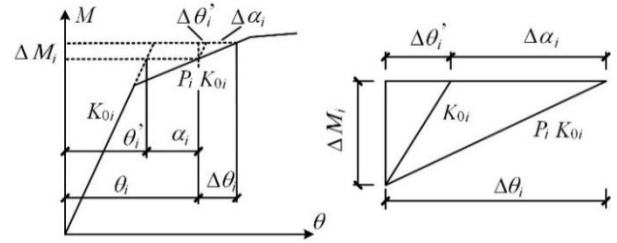


Fig. 4 Restoring force characteristics of the member

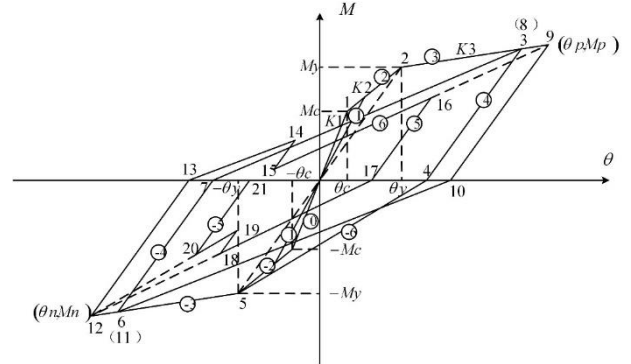


Fig. 5 Threefold line stiffness retrograde model of the member

$$\Delta\alpha_i = \frac{\Delta M_i}{P_i K_{0i}} - \frac{\Delta M_i}{K_{0i}} = \left(\frac{1 - P_i}{P_i} \right) \frac{\Delta M_i}{K_{0i}} \quad (4)$$

where P_i is the stiffness reduction coefficient.

Then substituting Eq. (4) into Eq. (3), the following equation can be obtained

$$\begin{aligned} \Delta M_i &= P_i K_{0i} \Delta\theta_i \\ \Delta\alpha_i &= (1 - P_i) \Delta\theta_i \end{aligned} \quad (5)$$

Similarly

$$\begin{aligned} \Delta M_j &= P_j K_{0j} \Delta\theta_j \\ \Delta\alpha_j &= (1 - P_j) \Delta\theta_j \end{aligned} \quad (6)$$

where, P_i and P_j are the stiffness reduction coefficients of the two ends of member in two bending direction.

The value of P_i and P_j is changing in the time history analysis procedure, they are adopted to change the stiffness of the member. In this paper, the stiffness reduction coefficient changes in the fold line path (Xu *et al.* 2003), as shown in Fig. 5. The cracking moment and yield moment of the members can be calculated according to the China seismic code, and then the member stiffness matrix at any time can be obtained according to the Threefold line stiffness retrograde model of the member.

When considering the space characteristics, the bending deformation in the XY plane is similar to the bending deformation in XZ plane, and then the relation between member end force and member end displacement of the elasto-plastic member can be expressed as

$$\{\Delta F\}^e = [k]^e \{\Delta\delta\}^e \quad (7)$$

where, $[k]^e$ is the elasto-plastic stiffness matrix of the member, $\{\Delta\delta\}^e$ is the displacement increment at the end of the member.

3.2 Arrangement and control strategy of MR dampers

MR dampers are usually installed between the column bracings of the structure, as shown in Fig. 6. The control force of each MR damper will be distributed to the four nodes connected to the MR damper. The distribution role is as following

$$U_i = U_{i+1} = U/2, \quad U_{i+2} = U_{i+3} = -U/2 \quad (8)$$

The classic LQR optimal control algorithm (Berkovitz 1974) is adopted to calculate the optimal control force of the MR dampers. However, the MR damper cannot provide the optimal control force computed by LQR optimal control algorithm due to the restriction of its minimum and maximum control forces. As we know, when there is no current input, the damper can be considered as a viscous fluid damper and provide the minimum force, when current is inputted to the damper and reaches magnetic saturation, it can provide the maximum control force. The minimum and maximum control forces are determined by the performance test in section 2.2, and the control strategy is adopted to obtain the control force provided by the MR dampers. Based on the above discussion, the following semi-active control strategy is adopted in this study

$$U_i = \begin{cases} U_{i,\max} \operatorname{sgn}(U_i) & U_i \cdot \dot{u}_i < 0 \text{ and } |U_i| > U_{i,\max} \\ U_i & U_i \cdot \dot{u}_i < 0 \text{ and } U_{i,\min} < |U_i| < U_{i,\max} \\ U_{i,\min} \operatorname{sgn}(U_i) & U_i \cdot \dot{u}_i > 0 \text{ or } |U_i| < U_{i,\min} \end{cases} \quad (9)$$

where, U_i , $U_{i,\max}$, $U_{i,\min}$, \dot{u}_i are the optimal control force, maximum control force, minimum control force and velocity of the i th damper.

Based on the above discussion, the general elasto-plastic dynamic analysis program of space frame structure incorporated with MR dampers is developed using MATLAB, and a numerical example is introduced to verify the effectiveness of the elasto-plastic dynamic analysis program.

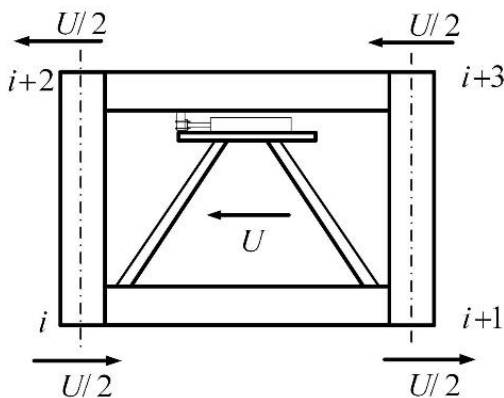


Fig. 6 Sketch of the MR damper location

3.3 Numerical example

A six story space frame structure is employed in this section, as shown in Fig. 7. The sizes of the beam and column are 0.3×0.6 m and 0.5×0.5 m, the cracking moment and yielding moment of the beam are 73 kN.m and 380 kN.m, the cracking moment and yield moment of the column are 88 kN.m and 300 kN.m.

Assuming that the columns do not subjected to any constant axial force. The Rayleigh orthogonal damping model is adopted here, in which the first two modal damping ratio are both 0.05. There are totally Six MR dampers installed in the first, second and third stories in the space frame structure, and two MR dampers are installed symmetrically in the XZ plane in each story. The El-Centro wave along the X direction is adopted as the seismic input, the duration and peak value of the wave is 30 s and 400 gal, and the time step is 0.02 s. *Newmark-β* method is chosen as the time history analysis method, the corresponding parameters are $\gamma=0.5$, $\beta=0.25$.

The dynamic responses of the structure under seismic excitations are shown in Figs. 8-9. Taking the dynamic responses of node 4 on the top floor for example, Fig. 8 shows the displacement and acceleration responses of the ideal optimal controlled, passive-off controlled and uncontrolled structure. It can be seen that both the displacement and acceleration responses of the ideal optimal controlled and passive-off controlled structure are reduced compared to the uncontrolled structure, the responses of the idea optimal controlled structure are reduced more effectively, especially the displacement

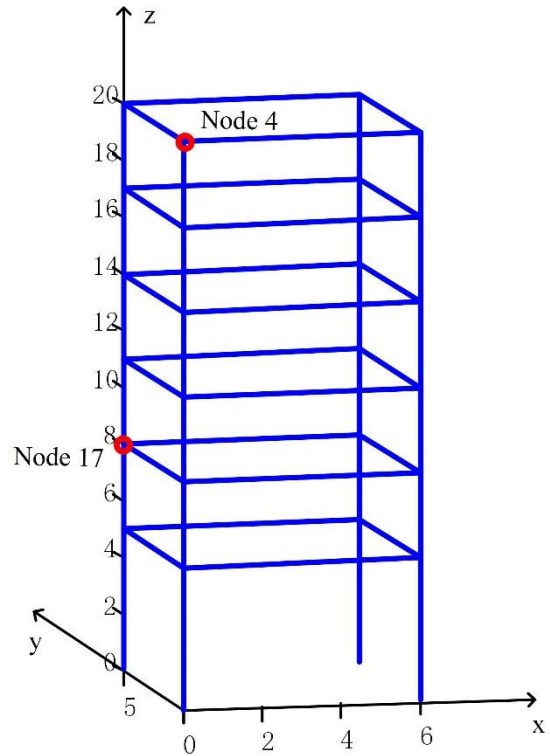


Fig. 7 Sketch of the space frame structure

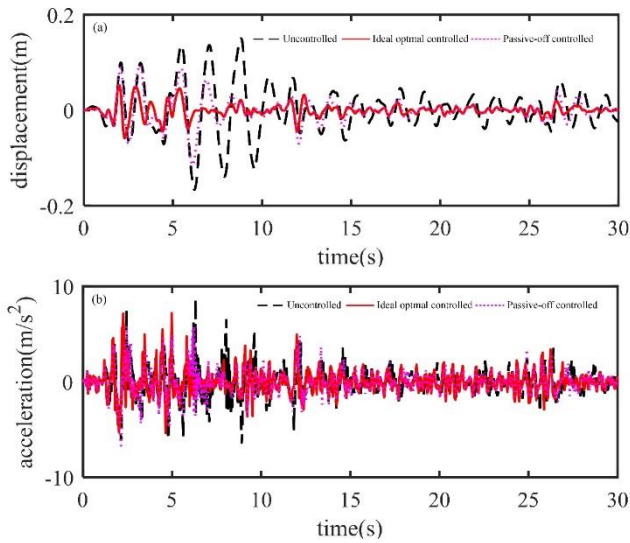


Fig. 8 Dynamic response history curves of node 4

response, which is significantly reduced. Specifically, Fig. 8(a) shows the displacement response, the maximum displacement response of the uncontrolled structure is 166.85 mm, the maximum displacement response of the passive-off controlled structure is 114.6 mm with a reduction of 31.32%, and the maximum displacement response of the ideal optimal controlled structure is 58.71 mm with a reduction of 64.81%. Fig. 8(b) shows the acceleration response, the maximum acceleration response of the uncontrolled structure is 8.74 m/s², the maximum acceleration response of the passive-off controlled structure is 6.68 m/s² with a reduction of 23.57%, and the maximum acceleration response of the controlled structure is 7.20 m/s² with a reduction of 17.62%. Results indicate that the MR damper can effectively mitigate the vibration energy and reduce the dynamic responses of the top story node of the structure.

The root mean square (RMS) of the responses of node 4 are also calculated and compared, as shown in Table 3. It can be seen that the displacement responses of the uncontrolled structure is 50.10 mm, while the 26.9 mm for the passive-off controlled structure with a reduction of 46.31% and 13.80mm for the ideal optimal control with a reduction of 72.46%. For the acceleration RMS responses, the uncontrolled structure is 1.49 m/s², while 1.31 m/s² for the passive-off controlled structure with a reduction of 12.08% and 1.25 m/s² for the ideal optimal controlled structure with a reduction of 16.11%.

Fig. 9 shows the acceleration and displacement responses of node 17 in the second floor of the ideal optimal controlled, passive-off controlled and uncontrolled structure, it can be seen that the displacement responses of the ideal optimal controlled and passive-off controlled structure are reduced significantly compared to the uncontrolled structure, while the acceleration response magnifies in a certain extent. Specifically, Fig. 9(a) shows the displacement responses, the maximum displacement response of the uncontrolled structure is 60.23 mm, the maximum displacement response of the passive-off

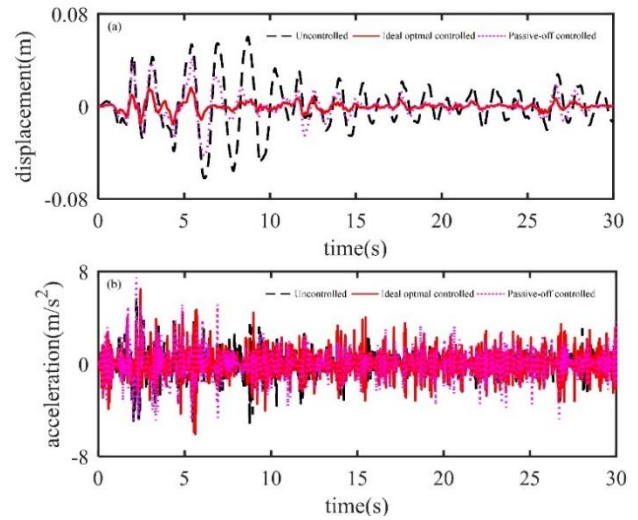


Fig. 9 Dynamic response history curves of node 17

controlled structure is 42.30 mm with a reduction of 29.77%, and the maximum displacement response of the controlled structure is 16.12 mm with a reduction of 73.24%. Fig. 9(b) shows the acceleration responses, the maximum acceleration response of the uncontrolled structure is 5.71 m/s², the maximum acceleration response of the passive-off controlled structure is 7.48 m/s² with a magnification of 31.00%, and the maximum acceleration response of the controlled structure is 6.47 m/s² with a magnification of 13.31%, the main reason is that MR dampers increased the stiffness of the stories which leads to the magnification of the acceleration response. Results indicate that MR dampers can effectively mitigate the vibration energy and reduce the displacement responses of the structure, while the acceleration response of the story which incorporated with MR damper will magnify to a certain extent.

The RMS of the responses of node 17 are also calculated and compared, as shown in Table 3. It can be seen that the displacement responses of the uncontrolled structure is 20.90 mm, while the 11.00 mm for the passive-off controlled structure with a reduction of 47.37% and 3.80mm for the ideal optimal control with a reduction of 81.82%. For the acceleration RMS responses, the uncontrolled structure is 1.14 m/s², while 1.24 m/s² for the passive-off controlled structure with a magnification of 8.77% and 1.22 m/s² for the ideal optimal controlled structure with a magnification of 7.02%.

Table 3 RMS value of the dynamics responses of Node 4 and Node 17

Control cases	Node 4		Node 17	
	Displacement (mm)	Acceleration (m/s ²)	Displacement (mm)	Acceleration (m/s ²)
Uncontrol	50.10	1.49	20.90	1.14
Passive-off control	26.90	1.31	11.00	1.24
Ideal optimal control	13.80	1.25	3.80	1.22

The above results indicate that the MR dampers can significantly reduce the displacement dynamic responses of the structure. The control effect of acceleration response is relatively inconspicuous, and even magnification phenomenon appears, which is not obvious. This is mainly due to the increase of the story stiffness caused by MR dampers. However, the installation location of the MR dampers will directly influence the control effect. At the same time, the MR damper is very expensive, and the number of MR dampers will directly dominate the cost. Thus both the arrangement and the required number of the MR dampers should be optimized to obtain good control effect and limit the cost within a certain range at the same time. The genetic algorithm is adopted to optimize the arrangement of MR dampers in the following section, and finally the optimal locations are obtained under different determinate number of MR dampers.

4. Location optimization analyses of MR dampers

In this section, the genetic algorithm is adopted to optimize the location of MR dampers under different determinate number of MR dampers. The number of MR dampers is a restriction condition, thus the improved genetic algorithm is adopted in order to solve the optimization problem with constraints, as seen in following.

4.1 Coding rules

Since there are six available stories to arrange MR dampers, the code length of each individual is chosen as six, and the binary notation set $\{0,1\}$ is adopted to encode the location information of MR dampers. If the value of the i th gen of an individual is 1, then it means that two MR dampers are installed symmetrically along the X direction in the XZ plane in this story. Similarly, 0 represents that there is no MR damper in this story. For example, individual 011000 represents that two MR dampers are installed in the second story and two MR dampers are installed in the third story at the same time. In order to solve the location optimization problem with fixed number of MR dampers, assuming that n represents the total number of stories to install MR dampers, x_i represents the value of the i th gen, then the following restraint condition are adopted

$$\sum_{j=1}^6 x_j = x_1 + x_2 + \dots + x_6 = n \quad (10)$$

4.2 Objective function

To evaluate the control effect of the MR dampers, the displacement and acceleration responses are usually chosen as an important index, they can reflect the safety and comfortable of a structure in a certain extent. In this section, the combination of displacement and acceleration responses are chosen as the objective function

$$Objv = \alpha \frac{u_{\max}}{u_{o\max}} + \beta \frac{a_{\max}}{a_{o\max}} \quad (14)$$

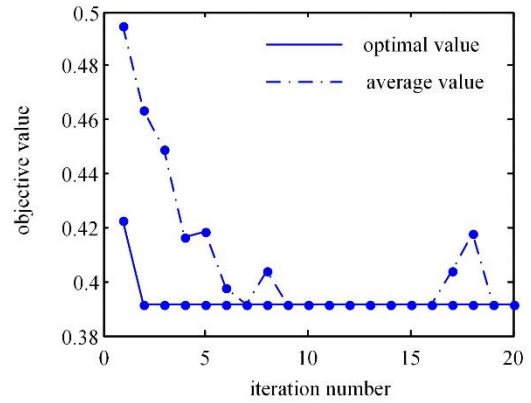


Fig. 10 Iterative process of genetic algorithm with eight dampers

where, u_{\max} and $u_{o\max}$ are the maximum displacement responses of node 4 of the controlled and uncontrolled structure, respectively. a_{\max} and $a_{o\max}$ are the maximum acceleration responses of node 4 of the controlled and uncontrolled structure, respectively. α and β are weighting coefficients.

4.3 Crossover and mutation

Due to the reason that the crossover and mutation process will lead to the variation of total number of MR dampers, the commonly used crossover and mutation method cannot meet the requirement of the optimization problem in this study. Thus the modified binary crossover and mutation method is adopted in this study to solve this problem, and the objective is to guarantee that the number of MR dampers of each individual maintains the same after crossover and mutation. As for crossover process, the main problem is converted to how to control the location of crossover points. For example, A and B are the parents individual,

A: 011010 B: 101100

Then there are three crossover points that can meet the requirement, they are points 2, 3 and 5, the MR damper number of each offspring individual will maintain the same if arbitrary point of the above three is chosen as the crossover point.

In the mutation procedure, we should also guarantee that the number of MR dampers maintains the same after mutation. Thus, if one gen is converted from 1 to 0, then there will be one gen converted from 0 to 1, similarly, if one gen is converted from 0 to 1, then there will be one gen converted from 1 to 0. Then the total number of MR dampers will maintain the same after mutation.

4.4 Results and analysis

Based on the previous discussion, the number of initial population is chosen as 10, termination iteration is 20. By using genetic algorithm, the optimal arrangements of MR dampers are obtained under different fixed numbers of MR dampers.

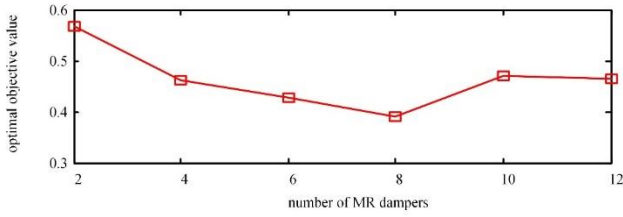


Fig. 11 Changing of objective value with increasing MR dampers

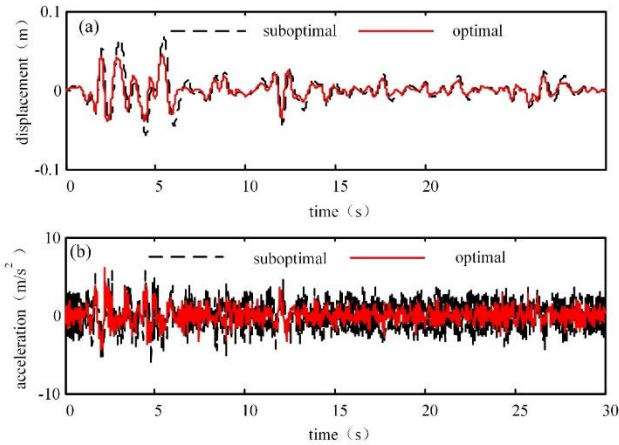


Fig. 12 Dynamic responses comparison of node 4 between optimal and suboptimal controlled structure

Taking the restraint of eight MR dampers are installed in the structure for example, Fig. 10 shows the varying process of optimal objective value and average objective value of the population with respect to iteration numbers. It can be seen that the genetic algorithm converges quickly, and the average value equals the optimal value in the seventh iteration. The optimal individual is 011110, which means that the eight MR dampers are located in the 2st, 3st, 4st and 5th story respectively, and the average value is reduced to 0.3918 from 0.4947 by optimization. Results show that the genetic algorithm can effectively optimize the arrangements of MR dampers and obtain better control effect.

The optimized arrangement results under different determinate number of MR dampers are listed in Table 4, the optimal location of MR dampers and the optimal objective value under different number of MR dampers are obtained. It can be seen that the optimal objective value decreases with increasing number of MR dampers at the beginning and then increase when the number of MR dampers exceeds eight, in order to illustrate the changing role more clearly, Fig. 11 shows the changing of objective value with increasing MR dampers. It can be seen that the optimal objective value is minimum when eight MR dampers are located in the second to fifth stories of the structure. Comparatively speaking, using the scheme of eight dampers to control the structural vibration is sensible.

In order to verify the effectiveness of optimization analysis more clearly, taking eight dampers for example, and the suboptimal locations of MR dampers are chosen arbitrarily, such as from the third to sixth stories.

Comparisons of the dynamic responses of node 4

Table 4 Location optimal results

Location restriction	Number of MR dampers	Optimal location	Optimal objective value
1	2	001000	0.5691
2	4	100100	0.4616
3	6	011010	0.4282
4	8	011110	0.3918
5	10	110111	0.4702
6	12	111111	0.4661

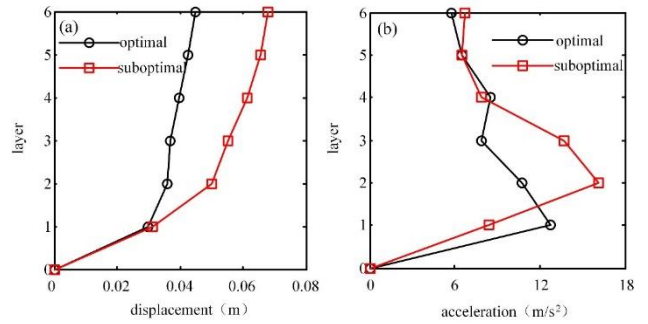


Fig. 13 Maximum dynamic responses of each story

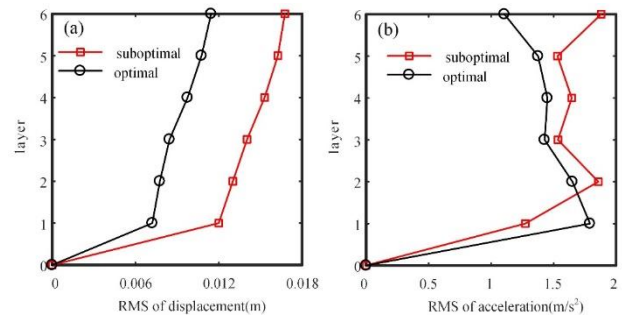


Fig. 14 Root mean square value of dynamic responses of each story

between the optimal and suboptimal controlled structure is shown in Fig. 12. It can be seen that both the displacement and acceleration responses are reduced, the peak value of the displacement and acceleration responses of the suboptimal controlled structure are 67.65 mm and 6.35 m/s², while the peak value of the optimal controlled structure are 44.71 mm and 5.96 m/s², with a reduction of 33.91% and 6.14%, respectively.

Fig. 13 shows the dynamic responses of each story of the structure, it can be seen that both the displacement and acceleration responses of the optimal controlled structure are mitigated more effectively compared with the suboptimal controlled structure. The peak values of the displacement and acceleration responses of the optimal controlled structure are reduced by 33.72% and 26.01%, respectively, compared with the suboptimal controlled structure.

Figs. 14(a)-(b) shows the RMS value of the displacement and acceleration responses of each story of the structure respectively, it can be seen that both the displacement and acceleration responses of the optimal

controlled structure are mitigated more effectively compared with the suboptimal controlled structure. Taking the top layer for example, the RMS value of the displacement and acceleration responses of the suboptimal controlled structure are 0.0168 m and 1.8805 m/s², and 0.0114 m and 1.1063 m/s² for the optimal controlled structure, which also shows that the dynamic responses of the optimal controlled structure are mitigated more effectively.

5. Conclusions

In this paper, performance tests on a MR damper are carried out, and the damping characteristics and energy dissipation capacity are analyzed. Then the control effect is evaluated through the dynamic responses of a six-story space frame structure by using the developed elasto-plastic dynamic analysis program. Finally, the locations of MR dampers are optimized by using the improved genetic algorithm, and the following conclusions can be obtained.

- The influence of excitation amplitude and frequency on the damping force is not distinct. While the damping force of the MR damper increases obviously with increasing currents and approaches magnetic saturation at nearly 2.4A, the saturation current is determined by both the magnetic circuit structure and the characteristics of the MR fluid used in the MR damper.
- The energy dissipation capacity of the MR damper increases obviously with increasing current and finally nearly maintains the same, energy dissipation capacity increases with increasing amplitude and almost maintains unchanged with increasing frequency.
- The elasto-plastic dynamic analysis program can effectively calculate the dynamic responses of the magnetorheological damping structure, and the MR damper can significantly reduce the dynamic responses of the structure.
- The genetic algorithm can optimize the location of MR dampers effectively and lead to a more significant control effect, and results indicate that using eight dampers arranged in the 2th, 3th, 4th and 5th floors can achieve the most optimal control effect. Considering the economical factor, using six dampers arranged in the 2th, 3th and 5th floors to mitigate seismic energy is also advisable.

Acknowledgments

The research described in this was financially supported by the National Science Fund for Distinguished Young Scholars (51625803); Natural Science Foundation of Jiangsu Province (BK20140025, BK20141086); Ten Thousand Talent Program (Scientific and technological innovation leader); A Project Funded by the Priority Academic Program Development of Jiangsu Higher Education Institutions (CE02-2-33); Research and Innovation Project for College Graduates of Jiangsu Province (KYLX15_0088), and the State Foundation for

Studying Abroad, China. These supports are gratefully acknowledged.

References

- Berovitz, L.D. (1974), *Optimal Control Theory*, Springer-Verlag, New York, NY, USA.
- Carlson, J.D., Catanzarite, D.M. and Clair, K.A. (1996), "Commercial magneto-rheological fluid devices", *Int. J. Modern Phys. B*, **10**(23-24), 2857-2865.
- Cetin, S., Zergeroglu, E., Sivrioglu, S. and Yuksek, I. (2011), "A new semiactive nonlinear adaptive controller for structures using MR damper: design and experimental validation", *Nonlinear Dyn.*, **66**(4), 731-743.
- Giberson, M.F. (1969), "Two nonlinear beams with definitions of ductility", *J. Struct. Div.*, **95**, 137-157.
- Jansen, L.M. and Dyke, S.J. (2000), "Semiactive control strategies for MR dampers: comparative study", *J. Eng. Mech.*, **126**(8), 795-803.
- Kim, Y., Langari, R. and Hurlebaus, S. (2009), "Semiactive nonlinear control of a building with a magnetorheological damper system", *Mech. Syst. Sign. Proc.*, **23**(2), 300-315.
- Lee, D.Y. and Wereley, N.M. (1999), "Quasi-steady Herschel-Bulkley analysis of electroand magneto-rheological flow mode dampers", *J. Intel. Mater. Syst. Struct.*, **10**(10), 761-769.
- Motra, G.B., Mallik, W. and Chandiramani, N.K. (2011), "Semi-active vibration control of connected buildings using magnetorheological dampers", *J. Intel. Mater. Syst. Struct.*, **22**(16), 1811-1827.
- Phillips, R.W. (1969), "Engineering applications of fluids with a variable yield stress", Ph.D. Dissertation, University of California, Berkeley.
- Soong, T.T. and Cimellaro, G.P. (2009), "Future directions in structural control", *Struct. Control Hlth. Monit.*, **16**(1), 7-16.
- Spencer, Jr. B.F., Dyke, S.J., Sain, M.K. and Carlson, J.D. (1997), "Phenomenological model for magnetorheological dampers", *J. Eng. Mech.*, **123**(3), 230-238.
- Tsang, H.H., Su, R.K.L. and Chandler, A.M. (2006), "Simplified inverse dynamics models for MR fluid dampers", *Eng. Struct.*, **28**(3), 327-341.
- Tu, J.W., Liu, J., Qu, W.L., Zhou, Q., Cheng, H.B. and Cheng, X.D. (2011), "Design and fabrication of 500-kN large-scale MR damper", *J. Intel. Mater. Syst. Struct.*, **22**(5), 475-487.
- Wang, X. and Gordaninejad, F. (1999), "Flow analysis of field-controllable, electro-and magneto-rheological fluids using Herschel-Bulkley model", *J. Intel. Mater. Syst. Struct.*, **10**(8), 601-608.
- Wereley, N.M. and Pang, L. (1998), "Nondimensional analysis of semi-active electrorheological and magnetorheological dampers using approximate parallel plate models", *Smart Mater. Struct.*, **7**(5), 732-743.
- Xu, Z.D. and Guo, Y.Q. (2006), "Fuzzy control method for earthquake mitigation structures with Magnetorheological dampers", *J. Intel. Mater. Syst. Struct.*, **17**(10), 871-881.
- Xu, Z.D., Jia, D.H. and Zhang, X.C. (2012), "Performance tests and mathematical model considering magnetic saturation for magnetorheological damper", *J. Intel. Mater. Syst. Struct.*, **23**(12), 1331-1349.
- Xu, Z.D. and Shen, Y.P. (2003), "Intelligent bi-state control for the structure with magnetorheological dampers", *J. Intel. Mater. Syst. Struct.*, **14**(1), 35-42.
- Xu, Z.D., Shen, Y.P. and Guo, Y.Q. (2003), "Semi-active control of structures incorporated with magnetorheological dampers using neural networks", *Smart Mater. Struct.*, **12**(1), 80-87.
- Xu, Z.D., Liao, Y.X., Ge, T. and Xu, C. (2016a), "Experimental

- and theoretical study of viscoelastic dampers with different matrix rubbers”, *J. Eng. Mech.*, **142**(8), 04016051.
- Xu, Z.D., Suo, S. and Lu, Y. (2016b), “Vibration control of platform structures with magnetorheological elastomer isolators based on an improved SAVS law”, *Smart Mater. Struct.*, **25**(6), 065002.
- Xu, Z.D., Xu, F.H. and Chen, X. (2016c), “Vibration suppression on a platform by using vibration isolation and mitigation devices”, *Nonlinear Dyn.*, **83**(3), 1341-1353
- Yan, W.M., Ji, J.B., Dong, B. and Ge, H.J. (2011), “Theoretical and experimental studies on a new reversible magnetorheological damper”, *Struct. Control Hlth. Monit.*, **18**(1), 1-19.
- Yang, G., Spencer, Jr. B.F., Carlson, J.D. and Sain, M.K. (2002), “Large-scale MR fluid dampers: modeling and dynamic performance considerations”, *Eng. Struct.*, **24**(3), 309-323.

CY